THE JOURNAL OF PHYSICAL CHEMISTRY C
A JOURNAL OF THE AMERICAN CHEMICAL SOCIETY

pubs.acs.org/JPCC

Article

Real-Space Observations of Multiple Reaction Pathways Enabled by Plasmonic Hot Carriers

Published as part of The Journal of Physical Chemistry C virtual special issue "Hot Electrons in Catalysis".

Emiko Kazuma, Minhui Lee, Jaehoon Jung, Michael Trenary, and Yousoo Kim*

Cite This: *J. Phys. Chem. C* 2023, 127, 10953−10959

Read Online

ACCESS | Metrics & More | Article Recommendations | Supporting Information

ABSTRACT: Plasmonic hot carriers generated by the decay of localized surface plasmons have the potential to enable chemical reactions at energies lower than those required for photochemical reactions as well as reactions impossible to achieve with light alone. A broad energy distribution of the hot carriers would enable multiple reaction pathways by the transfer of the hot carriers to molecular electronic states of different energies. However, it is difficult to distinguish reaction pathways by detecting products using conventional macroscopic methods, and the mechanistic details are still unclear. In this study, we demonstrate that multiple reaction pathways are available with plasmonic hot carriers on the basis of the real-space observation of molecular motions as well as dissociation of O_2 molecules chemisorbed on the Ag(110) surface using a scanning tunneling microscope. This real-space study at a single-molecule level reveals that plasmonic hot carriers enable multiple reaction pathways due to their broad energy distribution, allowing access to various adsorbate states.

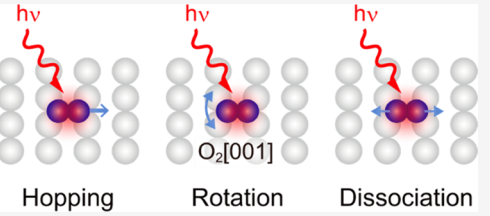

1. INTRODUCTION

Chemical reactions induced by localized surface plasmons are promising for the efficient use of solar energy because the plasmons not only enhance photochemical reactions but also enable reactions that are not possible with conventional light.[1−5] The plasmons generate a strong electric field, hot carriers, and localized heat during the excitation and decay process, all of which can interact with molecules, leading to reactions. In particular, the plasmonic hot carriers have broad energy distributions from the Fermi level (E_F) to the energy of the incident light both above and below the E_F.[6−9] The transfer of the plasmonic hot carriers to molecules can trigger chemical reactions at an energy lower than the energy required for the direct excitation of frontier orbitals.[10,11]

Various kinds of plasmon-induced chemical reactions, such as azo-bond formation, Suzuki−Miyaura coupling, and dissociation of H_2, O_2, NH_3, H_2O, H_2S, and C−C bonds, have been reported and interpreted by the hot-carrier transfer mechanism.[10−18] Although the transfer of hot carriers has been considered to be the main mechanism in plasmon-induced chemical reactions, the details of the interaction between the plasmonic hot carriers and molecular electronic states are still unclear.[4−6,19] It is generally accepted that the plasmonic hot carriers are transferred from the metal to the adsorbate states, and a transient charged state is formed, leading to a chemical reaction.[20] By considering the broad energy distribution of not only the plasmonic hot carriers but also of the adsorbate states originating from orbital hybridization between metal and molecular states at the interface, we expect that both electronic and vibrational excitation of molecules can be induced by the transfer of the plasmonic hot carriers, which leads to diverse reaction pathways. However, it is hard to discern multiple reaction pathways with conventional macroscopic methods by only detecting products. Moreover, molecular motions associated with vibrational and rotational excitation are difficult to detect. Even though experimental techniques to analyze chemical reactions induced by the plasmons are developing from ensemble measurements to single-particle and local measurements using probe techniques,[21,22] the details of the reaction mechanisms and the interaction of the plasmons with molecules are still unclear.

Real-space observation and analyses of chemical reactions at the location where plasmons are localized using a scanning tunneling microscope (STM) with a high spatial resolution is an effective approach to clarify the reaction pathways and mechanisms in detail.[23−27] In addition to observation, the STM can be applied to trace the chemical reactions of a single molecule in real time by monitoring the tunneling current.[23] A recent study achieved the precise control of bond dissociation inside a single molecule using a plasmon atomically confined at the STM junction.[26] Technical advances in STM, combined with noncontact atomic force microscopy and tip-enhanced

Received: March 22, 2023
Revised: May 13, 2023
Published: June 6, 2023

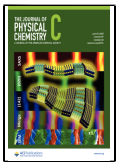

https://doi.org/10.1021/acs.jpcc.3c01916
J. Phys. Chem. C 2023, 127, 10953−10959

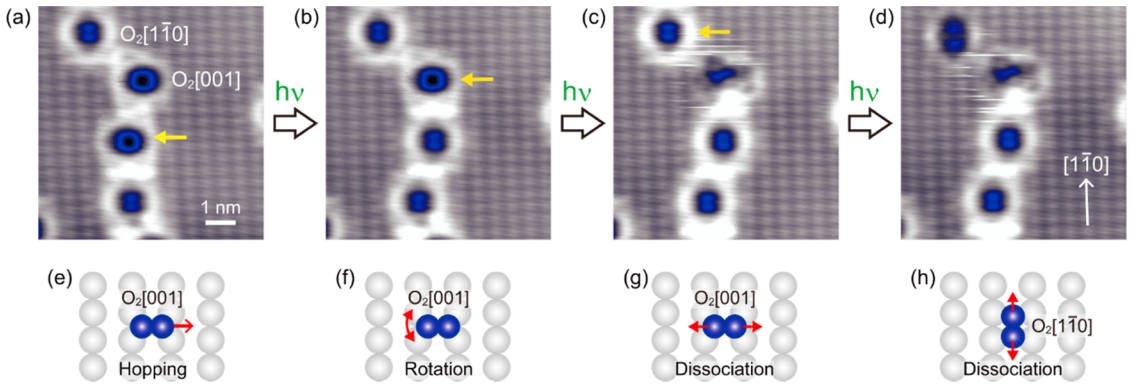

Figure 1. Atomically resolved topographic STM images of O_2 molecules on Ag(110) (a) before and (b–d) after irradiation with *p*-polarized light at 500 nm (2.6×10^{15} photons cm^{-2} s^{-1}, ~1.03 mW cm^{-2}) by using a Ag tip modified with a molecule/atom. A fixed gap resistance at 20 mV and 2.0 nA was applied, and the feedback loop was turned off to maintain the tip height during light irradiation. All STM images were obtained at 5 K in the dark, and the scanning condition was 20 mV and 0.2 nA. The Ag tip was positioned over the molecule, indicated by the yellow arrows in the STM images during light irradiation. (e–h) Schematic illustrations of (e) hopping, (f) rotation, and (g) dissociation of $O_2[001]$ and (h) dissociation of $O_2[1\bar{1}0]$.

Raman scattering, led to the detailed characterization of the chemical structure of a single molecule generated by the plasmon.[27] In our previous studies, we elucidated the mechanisms of dissociation reactions for dimethyl disulfide molecules adsorbed on Ag(111) and Cu(111) and O_2 molecules on Ag(110) based on single-molecule investigations using the STM.[23,24] In the case of dimethyl disulfide, the localized plasmonic field directly interacts with the molecule, namely, by direct intramolecular excitation, resulting in dissociation.[23] By contrast, oxygen molecules dissociate through the transfer of plasmonic hot carriers to the molecular states.[24] The efficiency of dissociation induced by hot-hole transfer was much larger than that induced by hot-electron transfer due to the anisotropic energy distribution near the E_F of the molecular electronic states strongly hybridized with the metal states.

In this study, multiple plasmon-induced reaction pathways of O_2 chemisorbed on Ag(110) were observed and analyzed with an STM at the single-molecule level. Rotational and hopping motions as well as dissociation reactions were observed only for O_2 molecules aligned along Ag[001] axis ($O_2[001]$). We revealed that the multiple reaction pathways were caused by the transfer of the plasmonic hot carriers with broad energy distributions to various molecular electronic states by comparing plasmon-induced reactions with reactions induced by injecting tunneling electrons/holes from the STM tip.

2. EXPERIMENTAL SECTION

2.1. Preparation of Samples and Plasmonic Tips. Atomically flat and clean surfaces of a single-crystalline Ag(110) substrate (MaTecK) were obtained by repeated cycles of Ar^+-ion sputtering and annealing at ~800 K. O_2 molecules were chemisorbed on the surface of the substrate kept on a cold stage maintained at 89 K by dosing O_2 molecules from a small gas cylinder filled with O_2 gas (purity > 99.99995 vol %) at room temperature. The prepared sample was moved to the STM head and cooled down to ~5 K. Plasmonic tips made of Ag/Au were prepared as previously reported.[23,28] The tip shape was evaluated from SEM images.

2.2. Optical Setup for STM Experiments with Light Irradiation. All experiments were performed using a low-temperature STM (Omicron GmbH) maintained at 5 K under an ultra-high vacuum of less than 4.0×10^{-11} Torr. The p-polarized light with an incident angle of 25° relative to the sample surface was introduced into the STM chamber through an optical window made of fused silica. The light source was a Xe lamp having a small emission size (~0.1 mm), which was directly coupled to the optical fiber (Laser-Driven Light Source, Tokyo Instruments, Inc). The light was concentrated by lenses attached outside the chamber and focused on the sample surface with a spot diameter of $\varphi \sim 1.6$ mm. Monochromatic light was extracted using a bandpass filter. The center wavelength (CWL) and full width at half-maximum (FWHM) of the bandpass filters (CWL, FWHM) were (500 nm, 10 nm), (600, 650, and 700 nm, 25 nm), (750 and 800 nm, 40 nm), and (900, 1000, 1100, 1200, and 1500 nm, 50 nm). Light intensity was tuned with neutral density filters and was evaluated in a position equivalent to that of the sample with all optical components in the path using an optical power meter and a dual scanning slit beam profiler (Thorlabs).

2.3. Single-Molecule Study of Reactions Induced by the Plasmon. An STM image of O_2 molecules on the Ag(110) surface was obtained before light irradiation. To investigate the plasmon-induced reaction, a plasmonic tip was positioned over a target molecule at a fixed tunneling gap resistance (V = 20 mV and I = 2.0 nA), and the feedback loop was turned off to maintain the tip height during light irradiation at a specific wavelength for a fixed length of time (45–75 s). We also monitored the current trace during this process. After light irradiation, the STM image was obtained at the same scanned area as before light irradiation.

3. RESULTS AND DISCUSSION

An atomically resolved STM image shows O_2 molecules chemisorbed on the Ag(110) surface in two orientations at the hollow site, $O_2[001]$ and $O_2[1\bar{1}0]$ (Figure 1a), by using a Ag tip modified with a molecule/atom, as observed in previous STM studies.[24,29,30] Figure 1a–d shows the atomically resolved STM images obtained before and after the excitation of the plasmons with a plasmonic tip that was positioned on a target molecule during light irradiation. In addition to the plasmon-induced dissociation of both $O_2[001]$ and $O_2[1\bar{1}0]$ reported in our previous study[24] (Figure 1c,d), we observed the rotation of

https://doi.org/10.1021/acs.jpcc.3c01916
J. Phys. Chem. C 2023, 127, 10953–10959

$O_2[001]$ to $O_2[1\bar{1}0]$ accompanied by hopping (Figure 1b). The sample bias was always kept at 20 mV during light irradiation, and scanning in the dark at this level of bias never induced molecular motion and reaction. Figure 1e–h shows schematic illustrations of plasmon-induced molecular motions and reactions observed with STM.

To examine molecular motions and reactions induced by plasmons, we performed a statistical analysis of the processes induced by plasmons excited with light at different wavelengths. The quantitative analysis of reaction time and efficiency for the plasmon-induced molecular motions and reactions under the STM tip is possible by monitoring the change in the tunneling current (Figure S1). However, the current change caused by rotational motion is occasionally too small to detect, which disables calculating the yield. We therefore analyzed the probabilities of dissociation, rotation, and hopping of a single molecule under the tip by counting the number of each event. The probability provides information on the preferred reaction pathway at a specific energy. Figure 2

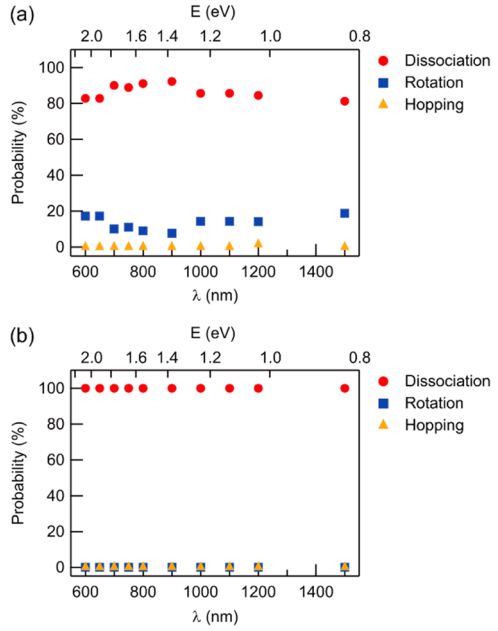

Figure 2. Probabilities of dissociation, rotation, and hopping for (a) $O_2[001]$ and (b) $O_2[1\bar{1}0]$ molecules induced by the plasmon excited at the nanogap between the Au tip and Ag(110) substrate as a function of light wavelength. A fixed gap resistance (20 mV and 2.0 nA) was applied, and the feedback loop was turned off to maintain the tip height during light irradiation. The probability is calculated from the ratio of the number of reacted molecules to the total number of trials at each wavelength. Each data point represents the average of 33 and 28 for (a) $O_2[001]$ and (b) $O_2[1\bar{1}0]$, respectively.

shows the probabilities of dissociation, rotation, and hopping for $O_2[001]$ and $O_2[1\bar{1}0]$ molecules induced by the plasmons excited at different wavelengths in the range of 600–1500 nm using a Au tip. Note that the resonance property of the plasmon at the nanogap between a Au tip and a Ag substrate was reported in our previous study.[24] For $O_2[001]$ molecules, not only dissociation but also rotation to $O_2[1\bar{1}0]$ and hopping were observed, although the probability of rotation and hopping were 8–19% and less than 1%, respectively (Figure 2a). On the other hand, for $O_2[1\bar{1}0]$ molecules, only dissociation occurred, and rotation and hopping were never observed at any wavelength (Figure 2b). In our previous study, we ruled out a thermal process caused by local heating by the plasmons at the low substrate temperature (~5 K) because of the linear increase in dissociation rate versus light intensity.[24] No change caused by light irradiation without a plasmonic tip was observed at ~5 K, ruling out a simple photochemical reaction. Furthermore, we also ruled out direct intramolecular excitation by the plasmon because the energy gap between occupied π and unoccupied π^* states was greater than 2 eV, whereas the peaks in the dissociation yields were around 1.6 eV.[24] Instead, we concluded that hot-carrier transfer is the most plausible mechanism based on the electronic structures responsible for the dissociation revealed by the combination of STM action spectroscopy and density functional theory (DFT) calculations.[24] We thus assumed that the rotation and hopping as well as dissociation were induced by hot-carrier transfer.

In the hot-carrier transfer mechanism, plasmonic hot carriers are transferred to a molecule via an inelastic tunneling process to form transient charged states,[20] which is an initial step leading to molecular motions and reactions. The investigation of molecular motions and reactions initiated from the transient charged states formed by charge transfer via the inelastic tunneling process in an STM would provide fundamental knowledge of the events caused by the transfer of plasmonic hot carriers. Thus, to confirm the reaction mechanism in detail, we investigated molecular motions and reactions and their probabilities induced by injecting tunneling electrons or holes from the STM tip and compared them with the behavior caused by the plasmon. Figure 3a–d shows STM images representing typical changes observed for $O_2[001]$ and $O_2[1\bar{1}0]$ molecules caused by injecting tunneling electrons or holes from an STM tip in the dark. In this experiment, we used a W tip instead of a plasmonic tip to avoid the excitation of a plasmon at the STM junction by applying high voltage.[31] As with the case of the plasmons, dissociation, rotation, and hopping were observed for $O_2[001]$, but only dissociation was observed for $O_2[1\bar{1}0]$ molecules. To obtain quantitative information on the reaction pathways, we analyzed the probabilities of dissociation, rotation, and hopping caused by injecting tunneling electrons or holes from the STM tip at different sample biases (Figure 4).

For $O_2[001]$ molecules, the bias dependence of the probabilities exhibits a similar tendency at both bias polarities (Figure 4a–c). The probabilities of dissociation, rotation, and hopping are different depending on the applied bias. The hopping probability is almost zero at higher bias regions and tends to increase as $|V|$ decreases but is still ~8% at −0.3V. The bias dependence of the probabilities of dissociation and rotation is not simple; their probabilities are almost constant at $|V| > 0.6$ V but become complicated in the lower energy region. The probability of dissociation is larger than that of rotation at $|V| = 0.3–0.4$ V. Even though the dissociation yield increases at $|V| = \sim 0.4$ V, as reported in our previous study,[30] the probabilities of dissociation and rotation decrease and increase from $|V| = 0.4$ V, respectively. This can be explained by the change of the excitation manner for rotation at ~0.4 V. The rotation is a more efficient reaction pathway that would be induced by one-step excitation because the energy barrier between $O_2[001]$ and $O_2[1\bar{1}0]$ was reported as ~0.4 to 0.45 V,[32,33] while dissociation needs two-step excitation in this energy region. However, at $|V| = \sim 0.5$ V, the probabilities of dissociation and rotation again increase and decrease as $|V|$ increases, respectively. Considering the dissociation barrier

https://doi.org/10.1021/acs.jpcc.3c01916
J. Phys. Chem. C 2023, 127, 10953–10959

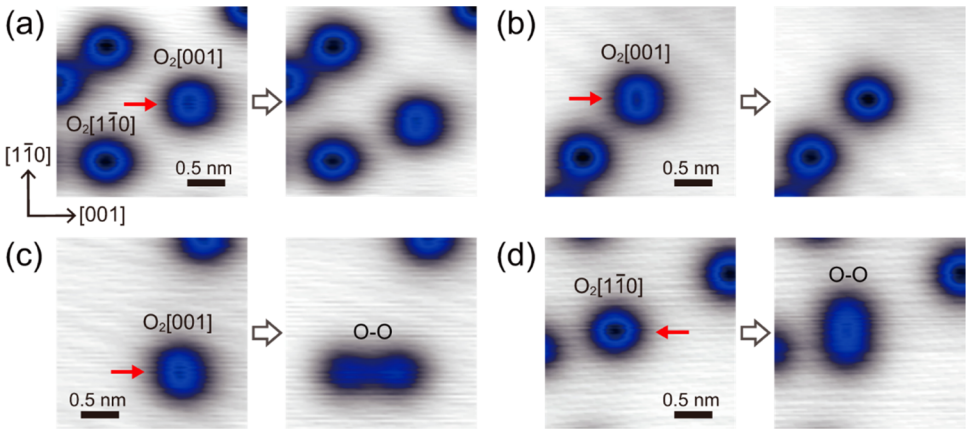

Figure 3. Typical topographic STM images of O_2 molecules on Ag(110) obtained with a W tip before and after (a) hopping, (b) rotation, and (c) dissociation of $O_2[001]$ and (d) dissociation of $O_2[1\bar{1}0]$ induced by applying a sample bias voltage pulse in the dark. Target molecules are indicated by red arrows in the STM images. The scanning condition was 20 mV and 0.2 nA.

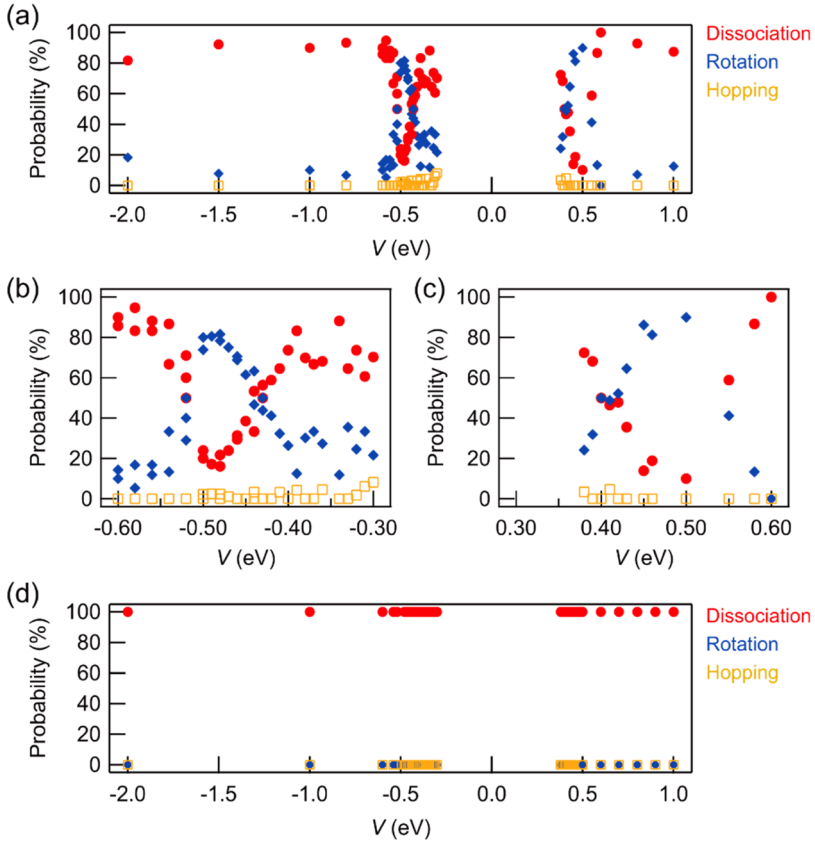

Figure 4. Probabilities for hopping, rotation, and dissociation for (a–c) $O_2[001]$ and (d) $O_2[1\bar{1}0]$ molecules as a function of sample bias voltage. The total numbers of trials are (a) 1637 and (d) 984, respectively. (b) and (c) are magnified data from (a) near the Fermi level in (b) negative and (c) positive bias regions.

(ε_{dis}) for $O_2[001]$, which was estimated to be $430 < \varepsilon_{dis} < 588$ meV,[30] the increase in the dissociation probability at $|V| = \sim 0.5$ V is interpreted as due to the change of process from two-step excitations of overtone-mediated channels for the O–O stretching mode to single-step excitation of the vibrational ladder or electronic excitation. At $|V| \geq 0.6$ V, the probabilities for all reaction pathways become almost constant, which means that electrons (or holes) broadly distributed from the E_F to the energy corresponding to the applied voltage are transferred to molecular states, leading to the excitation of all reaction pathways at a constant ratio.

In contrast to the complicated bias dependence of the probabilities due to the presence of three reaction pathways for $O_2[001]$, only dissociation was observed for $O_2[1\bar{1}0]$ molecules at any sample bias, as shown in Figure 4d. Previous studies reported that the chemisorption energy for $O_2[001]$ and $O_2[1\bar{1}0]$ are almost the same, and the simulated potential energy barrier between $O_2[001]$ and $O_2[1\bar{1}0]$ (ε_{rot}) is ~0.4 to 0.45 eV.[33] In our experiment, we observed only $O_2[1\bar{1}0]$ molecules when the substrate temperature is slightly higher than 90 K during O_2 exposure, but for substrate temperatures less than 90 K during O_2 exposure, both $O_2[001]$ and $O_2[1\bar{1}0]$

https://doi.org/10.1021/acs.jpcc.3c01916
J. Phys. Chem. C 2023, 127, 10953–10959

are adsorbed on the Ag(110) surface. This result indicates that $O_2[1\bar{1}0]$ is slightly more thermodynamically stable than $O_2[001]$. In addition, the dissociation barrier for $O_2[1\bar{1}0]$ was estimated to be $456 < \varepsilon_{dis} < 640$ meV.[30] By considering these results, we can draw a potential energy surface, including dissociation and rotational motion, as shown in Figure 5. In the

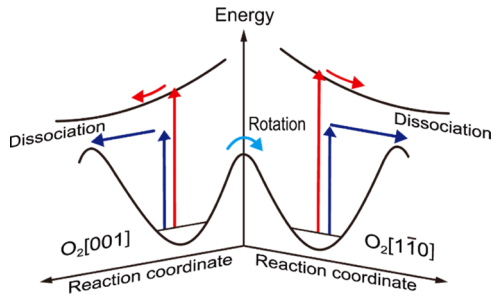

Figure 5. Schematic illustration of the potential energy surface for the dissociation and rotation of $O_2[001]$ and $O_2[1\bar{1}0]$. The dissociation barrier (ε_{dis}) is $430 < \varepsilon_{dis} < 588$ meV and $456 < \varepsilon_{dis} < 640$ meV for $O_2[001]$ and $O_2[1\bar{1}0]$, respectively.[30] Red and blue arrows indicate the dissociation pathway through the electronic excited states and vibrational excited states, respectively. Light blue indicates the rotation pathway from $O_2[001]$ to $O_2[1\bar{1}0]$.

case of $O_2[001]$, dissociation and rotation competitively occur, indicating that both dissociation and rotational pathways are available according to the potential energy surface. By contrast, the experimental result that only the dissociation pathway is allowed for $O_2[1\bar{1}0]$ even at low energies cannot be explained only by the difference of energy barriers for dissociation and rotation. The possible explanation is the difference in the electronic structure of the two chemisorption states caused by the difference in the distribution of the π orbital,[34,35] which results in a different manner for the excitation of rotation or the mode coupling between vibration and rotation, or the change of the lifetime of the vibrationally excited state responsible for the corresponding molecular motion.

Molecular motions and reactions for both $O_2[001]$ and $O_2[1\bar{1}0]$ caused by the plasmons are the same as those initiated by injecting tunneling electrons and holes from the STM tip. This indicates that hot-carrier transfer in which the hot carriers are transferred to the electronic states of adsorbed molecules leading to chemical reactions is the most plausible mechanism. The energy of the plasmonic hot carriers immediately after the excitation of the plasmons is broadly distributed from the E_F to the energy of the incident light and the distribution changes due to the energy decay with time.[7,36,37] Their broad energy distribution allows access to various molecular electronic states via inelastic tunneling of the plasmonic hot carriers to molecular states aligned at the same energy level. Therefore, three pathways, dissociation, rotation, and hopping, are available for $O_2[001]$. The observation of hopping motion caused by the plasmons especially provides evidence that plasmonic hot carriers with not only high energies but also low energies generated through the plasmon decay also contribute to molecular motions and reactions. By contrast, in our previous study, rotational motion induced by the plasmons was never observed for dimethyl disulfide molecules on Ag(111) in which plasmon-induced dissociation occurs not through hot-carrier transfer but through direct intramolecular excitation.[23] This also implies that the hot carriers are more accessible to various excitation pathways owing to their broad energy distribution, unlike direct excitation, including the intramolecular excitation and excitation between metal and adsorbate states, in which the exact energy matching between the plasmons and excitation pathways is necessary. The experimental result that only dissociation was observed for $O_2[1\bar{1}0]$ reveals that the reaction pathways accessible with the plasmonic hot carriers are governed by the potential energy surface derived from intrinsic adsorbate electronic states (Figure 5). The big change in potential that could alter the reaction pathways due to strong light coupling[38−40] would not be expected under our experimental conditions using a light intensity comparable to that of sunlight.

4. CONCLUSIONS

We revealed that plasmonic hot carriers enable multiple reaction pathways, including dissociation, hopping, and rotation, for O_2 molecules chemisorbed on the Ag(110) surface by the real-space investigation using STM at the single-molecule level. The emergence of multiple reaction pathways can be explained by the transfer of the plasmonic hot carriers with a broad energy distribution to the adsorbate states. We also found that the available reaction pathways depend on the adsorption orientations of the O_2 molecules and are governed by the intrinsic potential energy surfaces without significant perturbation by the plasmons under our experimental conditions. These findings could pave the way for designing plasmonic catalysts to access various reaction pathways.

■ ASSOCIATED CONTENT

Supporting Information

The Supporting Information is available free of charge at https://pubs.acs.org/doi/10.1021/acs.jpcc.3c01916.

Current trace measurements for detecting an event caused by plasmon excitation and corresponding STM images in Figure S1 (PDF)

■ AUTHOR INFORMATION

Corresponding Author

Yousoo Kim − *Department of Applied Chemistry, School of Engineering, The University of Tokyo, Tokyo 113-8656, Japan; Surface and Interface Science Laboratory, RIKEN, Wako, Saitama 351-0198, Japan;* orcid.org/0000-0001-7730-0704; Email: ykim@riken.jp

Authors

Emiko Kazuma − *Department of Applied Chemistry, School of Engineering, The University of Tokyo, Tokyo 113-8656, Japan; Surface and Interface Science Laboratory, RIKEN, Wako, Saitama 351-0198, Japan;* orcid.org/0000-0003-0834-9832

Minhui Lee − *Department of Applied Chemistry, School of Engineering, The University of Tokyo, Tokyo 113-8656, Japan; Surface and Interface Science Laboratory, RIKEN, Wako, Saitama 351-0198, Japan;* orcid.org/0000-0001-7217-5334

Jaehoon Jung − *Department of Chemistry, University of Ulsan, Ulsan 44776, Republic of Korea;* orcid.org/0000-0001-6550-139X

Michael Trenary − *Department of Chemistry, University of Illinois Chicago, Chicago, Illinois 60607, United States;* orcid.org/0000-0003-1419-9252

Complete contact information is available at:
https://pubs.acs.org/10.1021/acs.jpcc.3c01916

Notes

The authors declare no competing financial interest.

■ ACKNOWLEDGMENTS

The present work was supported by KAKENHI (22H00286 and 22H04967). J.J. acknowledges the financial support of the National Research Foundation of Korea (NRF-2021R1A2C1009191). M.T. acknowledges support from a grant from the US National Science Foundation (CHE-2102622). The authors are grateful for the use of the HOKUSAI-BigWaterfall supercomputer system of RIKEN.

■ REFERENCES

(1) Linic, S.; Chavez, S.; Elias, E. Flow and Extraction of Energy and Charge Carriers in Hybrid Plasmonic Nanostructures. *Nat. Mater.* **2021**, *20*, 916−924.
(2) Narang, P.; Sundararaman, R.; Atwater, H. A. Plasmonic Hot Carrier Dynamics in Solid-State and Chemical Systems for Energy Conversion. *Nanophotonics* **2016**, *5*, 96−111.
(3) Zhang, Y.; He, S.; Guo, W.; Hu, Y.; Huang, J.; Mulcahy, J. R.; Wei, W. D. Surface-Plasmon-Driven Hot Electron Photochemistry. *Chem. Rev.* **2018**, *118*, 2927−2954.
(4) Cortés, E.; Besteiro, L. V.; Alabastri, A.; Baldi, A.; Tagliabue, G.; Demetriadou, A.; Narang, P. Challenges in Plasmonic Catalysis. *ACS Nano* **2020**, *14*, 16202−16219.
(5) Kazuma, E.; Kim, Y. Mechanistic Studies of Plasmon Chemistry on Metal Catalysts. *Angew. Chem., Int. Ed.* **2019**, *58*, 4800−4808.
(6) Brongersma, M. L.; Halas, N. J.; Nordlander, P. Plasmon-Induced Hot Carrier Science and Technology. *Nat. Nanotechnol.* **2015**, *10*, 25−34.
(7) Manjavacas, A.; Liu, J. G.; Kulkarni, V.; Nordlander, P. Plasmon-Induced Hot Carriers in Metallic Nanoparticles. *ACS Nano* **2014**, *8*, 7630−7638.
(8) Bernardi, M.; Mustafa, J.; Neaton, J. B.; Louie, S. G. Theory and Computation of Hot Carriers Generated by Surface Plasmon Polaritons in Noble Metals. *Nat. Commun.* **2015**, *6*, No. 7044.
(9) Brown, A. M.; Sundararaman, R.; Narang, P.; Goddard, W. A., III; Atwater, H. A. Nonradiative Plasmon Decay and Hot Carrier Dynamics: Effects of Phonons, Surfaces, and Geometry. *ACS Nano* **2016**, *10*, 957−966.
(10) Christopher, P.; Xin, H.; Linic, S. Visible-Light-Enhanced Catalytic Oxidation Reactions on Plasmonic Silver Nanostructures. *Nat. Chem.* **2011**, *3*, 467−472.
(11) Mukherjee, S.; Libisch, F.; Large, N.; Neumann, O.; Brown, L. V.; Cheng, J.; Lassiter, J. B.; Carter, E. A.; Nordlander, P.; Halas, N. J. Hot Electrons Do the Impossible: Plasmon-Induced Dissociation of H_2 on Au. *Nano Lett.* **2013**, *13*, 240−247.
(12) Huang, Y.-F.; Zhu, H.-P.; Liu, G.-K.; Wu, D.-Y.; Ren, B.; Tian, Z.-Q. When the Signal Is Not from the Original Molecule To Be Detected: Chemical Transformation of para-Aminothiophenol on Ag during the SERS Measurement. *J. Am. Chem. Soc.* **2010**, *132*, 9244−9246.
(13) Wang, F.; Li, C. H.; Chen, H. J.; Jiang, R. B.; Sun, L. D.; Li, Q.; Wang, J. F.; Yu, J. C.; Yan, C. H. Plasmonic Harvesting of Light Energy for Suzuki Coupling Reactions. *J. Am. Chem. Soc.* **2013**, *135*, 5588−5601.
(14) Zhou, L.; Zhang, C.; McClain, Mj.; Manjavacas, A.; Krauter, C. M.; Tian, S.; Berg, F.; Everitt, H. O.; Carter, E. A.; Nordlander, P.; Halas, N. J. Aluminum Nanocrystals as a Plasmonic Photocatalyst for Hydrogen Dissociation. *Nano Lett.* **2016**, *16*, 1478−1484.
(15) Yuan, Y.; Zhou, L.; Robatjazi, H.; Bao, J. L.; Zhou, J.; Bayles, A.; Yuan, L.; Lou, M.; Lou, M.; Khatiwada, S.; et al. Earth-Abundant Photocatalyst for H_2 Generation from NH_3 with Light-Emitting Diode Illumination. *Science* **2022**, *378*, 889−893.
(16) Zheng, Z.; Tachikawa, T.; Majima, T. Single-Particle Study of Pt-Modified Au Nanorods for Plasmon-Enhanced Hydrogen Generation in Visible to Near-Infrared Region. *J. Am. Chem. Soc.* **2014**, *136*, 6870−6873.
(17) Lou, M.; Lou, M.; Bao, J. L.; Zhou, L.; Naidu, G. N.; Robatjazi, H.; Bayles, A. I.; Everitt, H. O.; Nordlander, P.; Carter, E. A.; et al. Direct H_2S Decomposition by Plasmonic Photocatalysis: Efficient Remediation plus Sustainable Hydrogen Production. *ACS Energy Lett.* **2022**, *7*, 3666−3674.
(18) Huh, H.; Trinh, H. D.; Lee, D.; Yoon, S. How Does a Plasmon-Induced Hot Charge Carrier Break a C−C Bond? *ACS Appl. Mater. Interfaces* **2019**, *11*, 24715−24724.
(19) Sánchez, C. G.; Berdakin, M. Plasmon-Induced Hot Carriers: An Atomistic Perspective of the First Tens of Femtoseconds. *J. Phys. Chem. C* **2022**, *126*, 10015−10023.
(20) Linic, S.; Aslam, U.; Boerigter, C.; Morabito, M. Photochemical Transformations on Plasmonic Metal Nanoparticles. *Nat. Mater.* **2015**, *14*, 567−576.
(21) Willets, K. A.; Wilson, A. J.; Sundaresan, V.; Joshi, P. B. Super-Resolution Imaging and Plasmonics. *Chem. Rev.* **2017**, *117*, 7538−7582.
(22) Cortés, E.; Grzeschik, R.; Maier, S. A.; Schlücker, S. Experimental Characterization Techniques for Plasmon-Assisted Chemistry. *Nat. Rev. Chem.* **2022**, *6*, 259−274.
(23) Kazuma, E.; Jung, J.; Ueba, H.; Trenary, M.; Kim, Y. Real-Space and Real-Time Observation of a Plasmon-Induced Chemical Reaction of a Single Molecule. *Science* **2018**, *360*, 521−526.
(24) Kazuma, E.; Lee, M.; Jung, J.; Trenary, M.; Kim, Y. Single-Molecule Study of a Plasmon-Induced Reaction for a Strongly Chemisorbed Molecule. *Angew. Chem., Int. Ed.* **2020**, *59*, 7960−7966.
(25) Böckmann, H.; Gawinkowski, S.; Waluk, J.; Raschke, M. B.; Wolf, M.; Kumagai, T. Near-Field Enhanced Photochemistry of Single Molecules in a Scanning Tunneling Microscope Junction. *Nano Lett.* **2018**, *18*, 152−157.
(26) Mahapatra, S.; Schultz, J. F.; Li, L.; Zhang, X.; Jiang, N. Controlling Localized Plasmons via an Atomistic Approach: Attainment of Site-Selective Activation inside a Single Molecule. *J. Am. Chem. Soc.* **2022**, *144*, 2051−2055.
(27) Xu, J.; Zhu, X.; Tan, S.; Zhang, Y.; Li, B.; Tian, Y.; Shan, H.; Cui, X.; Zhao, A.; Dong, Z.; et al. Determining Structural and Chemical Heterogeneities of Surface Species at the Single-Bond Limit. *Science* **2021**, *371*, 818−822.
(28) Yang, B.; Kazuma, E.; Yokota, Y.; Kim, Y. Fabrication of Sharp Gold Tips by Three-Electrode Electrochemical Etching with High Controllability and Reproducibility. *J. Phys. Chem. C* **2018**, *122*, 16950−16955.
(29) Hahn, J. R.; Ho, W. Orbital Specific Chemistry: Controlling the Pathway in Single-Molecule Dissociation. *J. Chem. Phys.* **2005**, *122*, No. 244704.
(30) Lee, M.; Kazuma, E.; Zhang, C.; Trenary, M.; Takeya, J.; Jung, J.; Kim, Y. Dissociation Mechanism of a Single O_2 Molecule Chemisorbed on Ag(110). *J. Phys. Chem. Lett.* **2021**, *12*, 9868−9873.
(31) Imada, H.; Miwa, K.; Imai-Imada, M.; Kawahara, S.; Kimura, K.; Kim, Y. Single-Molecule Investigation of Energy Dynamics in a Coupled Plasmon-Exciton System. *Phys. Rev. Lett.* **2017**, *119*, No. 013901.
(32) Olsson, F. E.; Lorente, N.; Persson, M. STM Images of Molecularly and Atomically Chemisorbed Oxygen on Silver. *Surf. Sci.* **2003**, *522*, L27−L35.
(33) Roy, S.; Mujica, V.; Ratner, M. A. Chemistry at Molecular Junctions: Rotation and Dissociation of O_2 on the Ag(110) Surface Induced by a Scanning Tunneling Microscope. *J. Chem. Phys.* **2013**, *139*, No. 074702.
(34) Alducin, M.; Sánchez-Portal, D.; Arnau, A.; Lorente, N. Mixed-Valency Signature in Vibrational Inelastic Electron Tunneling Spectroscopy. *Phys. Rev. Lett.* **2010**, *104*, No. 136101.
(35) Monturet, S.; Alducin, M.; Lorente, N. Role of Molecular Electronic Structure in Inelastic Electron Tunneling Spectroscopy: O_2 on Ag(110). *Phys. Rev. B* **2010**, *82*, No. 085447.

(36) Zhang, Y. Theory of Plasmonic Hot-Carrier Generation and Relaxation. *J. Phys. Chem. A* **2021**, *125*, 9201−9208.
(37) Jain, P. K.; Qian, W.; El-Sayed, M. A. Ultrafast Electron Relaxation Dynamics in Coupled Metal Nanoparticles in Aggregates. *J. Phys. Chem. B* **2006**, *110*, 136−142.
(38) Flick, J.; Rivera, N.; Narang, P. Strong Light-Matter Coupling in Quantum Chemistry and Quantum Photonics. *Nanophotonics* **2018**, *7*, 1479−1501.
(39) Bitton, O.; Gupta, S. N.; Haran, G. Quantum Dot Plasmonics: from Weak to Strong Coupling. *Nanophotonics* **2019**, *8*, 559−575.
(40) Garcia-Vidal, F. J.; Ciuti, C.; Ebbesen, T. W. Manipulating Matter by Strong Coupling to Vacuum Fields. *Science* **2021**, *373*, No. 178.

https://doi.org/10.1021/acs.jpcc.3c01916
J. Phys. Chem. C 2023, 127, 10953−10959